Characterization of interparticle forces in the packing of cohesive fine particles

R. Y. Yang,[1,*] R. P. Zou,[1] A. B. Yu,[1] and S. K. Choi[2]
[1]*Lab for Simulation and Modelling of Particulate Systems, School of Materials Science and Engineering, University of New South Wales, Sydney, New South Wales 2052, Australia*
[2]*Division of Petroleum Resources, CSIRO, Clayton, Victoria 3168, Australia*
(Received 14 April 2008; published 5 September 2008)

We numerically investigate force structures in the packing of fine cohesive particles using the discrete element method. By changing the particle size and therefore the van der Waals force, the effect of cohesion on the normal contact force and the total normal force, which is the sum of the normal contact forces and the van der Waals forces, is analyzed. It is shown that, with decreasing particle size, the normal contact forces become more uniform and have a narrower and more symmetric distribution, while the distributions of the total normal forces widen. Spatial correlation between the interparticle forces exists for the packing of coarse noncohesive particles. As the particle size decreases, this correlation becomes weaker for the contact forces but stronger for the total normal forces. A comparison between the effective weight of particles and the internal force structure suggests that there are differences between the particle-particle and particle-wall forces. The bimodal distribution of the effective weight indicates that there may exist two phases in the packings when cohesion is present, governed by the compressive and tensile stresses.

DOI: 10.1103/PhysRevE.78.031302 PACS number(s): 81.05.Rm, 61.43.Gt, 61.43.Bn

I. INTRODUCTION

Granular materials behave differently from other states of matter [1–3]. One unique yet still not fully understood feature of granular materials is the highly heterogeneous stress distribution in a homogeneous geometrical structure. When an external force (e.g., gravity or pressure) is applied to a particle assembly, the force does not propagate uniformly within the assembly, but along so-called "force chains" which define the path of interparticle forces. Such stress networks have been observed in both physical experiments [4–9] and numerical simulations [10–14]. Most results indicated that the force distribution $P(f)$ has an exponential falloff at large forces, although some results suggested the gradual movement of large forces from exponential to Gaussian form for particles with larger deformations [15–17]. Distributions at small forces are more uncertain. While some results showed that $P(f)$ has a small peak near the mean value and then decreases toward zero [4,7,11], others showed a plateau around the mean value and a slight increase with decreasing force [5,12]. Several explanations have been proposed, generally attributing this divergence to the sliding friction of the particles, which is history dependent [12,18]. Several theoretical models [16,19,20] have been proposed to explain this unique characteristic. More recently, the force distribution has also been linked to jammed systems [21–23]. For example, O'Hern *et al.* [23] observed in their simulation of supercooled liquids that a peak developed when the liquid was cooled down into a glass. They linked this feature with the development of a yield stress, which is regarded as the signature of jamming.

While there are numerous studies on the force distribution of noncohesive particles, only limited work has been done for particulate systems where cohesive interparticle forces are present and play a dominant role, as in the packing of fine or wet particles. Unlike systems of noncohesive particles, which are usually driven into a jammed state by externally applied stress, cohesive particles can evolve into a much looser jammed state as a result of the cohesive interparticle forces themselves, such as the capillary or van der Waals force [24]. This means the cohesive forces introduce another mechanism (tensile stress) in addition to the compressive stress. Therefore the packings of cohesive particles show more complicated internal force structures, which require more detailed and systematic studies. Trappe *et al.* [24] investigated attractive colloidal particles with a range of different interparticle interactions. They observed that, with larger interparticle forces, the large force network can span the system at lower packing densities. They also suggested that attractive colloid systems might provide a useful system with which to probe these force chains directly. Richefeu *et al.* [25] investigated the internal stress transmission in wet particles subjected to isotropic compaction. Their analysis of pressure on individual particles suggested that the packing is separated into tensile and compressive phases. On the other hand, Gilabert *et al.* [26] presented a two-dimensional simulation of the packing of particles with a short-range attraction under weak compaction. They observed that, with growing external pressure, the more localized force clusters evolved into force chains.

However, a qualitative study of the force structure in the packing of fine particles at the microscopic level is still lacking. We recently investigated the packing of cohesive particles (fine or wet) using the discrete element method (DEM) and studied the effect of the cohesive forces on the packing structure [27–29]. But our previous studies did not address how cohesion affects the force structure. There are questions still not properly answered yet: How do the interparticle forces evolve with cohesion? Can the force chain still be observed in packings with strong cohesion between particles? Are the forces spatially correlated under the effect of cohesion? All these questions are fundamentally important

*Corresponding author. r.yang@unsw.edu.au

and require systematic investigation. To answer these questions, we here extend our previous efforts by quantifying the force network in the packing of fine particles formed under gravity. Our analysis is mainly focused on the effect of cohesion between particles which is represented by the van der Waals force.

II. DEM MODEL AND SIMULATION CONDITIONS

The numerical DEM model used for the present work is the same as that used in our previous work [27]. In brief, the model treats a granular material as an assembly of discrete particles with each described by Newton's laws of motion, given by

$$m_i \frac{d\mathbf{v}_i}{dt} = \sum_j (\mathbf{F}_{n,ij} + \mathbf{F}_{s,ij} + \mathbf{F}_{v,ij}) + m_i \mathbf{g}, \tag{1}$$

$$I_i \frac{d\boldsymbol{\omega}_i}{dt} = \sum_j (\mathbf{R}_i \times \mathbf{F}_{s,ij} - \mu_r R_i |\mathbf{F}_{n,ij}| \hat{\boldsymbol{\omega}}_i), \tag{2}$$

where $\mathbf{v}_i$, $\boldsymbol{\omega}_i$, and I_i are, respectively, the translational and angular velocities and the moment of inertia of particle i; and $\hat{\boldsymbol{\omega}}_i = \boldsymbol{\omega}_i / |\boldsymbol{\omega}_i|$. $\mathbf{F}_{n,ij}$, $\mathbf{F}_{s,ij}$, and $\mathbf{F}_{v,ij}$ represent, respectively, the normal contact force, tangential contact force, and van der Waals force imposed on particle i by particle j. The detailed description of these forces can be found in our previous papers [27]. These force models have been demonstrated to be able to generate packings of particles comparable to experimental ones [27].

All simulations started with the random generation of monosized particles with no overlap in a rectangular container of size $15d \times 15d$. Then the particles were allowed to fall down under gravity while all the interparticle forces considered are effective, and finally the system came to rest to form a stable packing. Periodic boundary conditions were applied in the horizontal directions to eliminate, the effect of the wall. 5000 monosized particles were used in each simulation. Note that while the particle size was varied from 5 to 1000 μm for different simulations, the Hamaker constant of the particles was the same. The maximum van der Waals forces between particles ranged from 162.5 nN for 5 μm particles to 32.5 μN for 1000 μm particles. This gives a ratio of the van der Waals force to the gravity force varying from around 10^5 for 5 μm particles to 2.5 for 1000 μm particles. Table I lists the parameters used in the simulations. Unless otherwise stated, the values in the table are used in the following discussion.

TABLE I. Physical parameters in the simulation.

Parameter	Value
Particle size d	5–1000 μm
Particle density ρ	2.5×10^3 kg m^{-3}
Young's modulus Y	2.0×10^7 N m^{-2}
Poisson's ratio $\tilde{\sigma}$	0.29
Sliding friction coefficient μ	0.3
Rolling friction coefficient μ_r	0.005
Normal damping coefficient γ_n	5×10^{-6} s^{-1}
Hamaker constant H_a	6.5×10^{-20} J
Minimum separation $s_{\min}$	1 nm

III. RESULTS AND DISCUSSION

In contrast to the packing of noncohesive particles, in which only repulsive contact forces are present between particles, the interparticle forces in the packing of fine particles include the attractive van der Waals force as well as the repulsive Hertzian force. So when two particles have interaction, the net interparticle force in the normal direction should be the sum of the normal contact force and the van der Waals force. The following section will mainly focus on the contact force F_c and the total normal interparticle force F_n, which is the sum of F_c and the van der Waals force F_v.

Figure 1 shows the spatial distributions of F_c and F_n in the packings of different sized particles. The F_c network in the packing of 1 mm particles [Fig. 1(a)] clearly shows force gradients along the gravity direction with the larger force at the bottom propagating upward to support the weight of particles above. With decreasing particle size, the van der Waals force gradually takes over from gravity as the dominant force. So the systems are jammed at much looser states, and the contact forces between particles mainly counterbalance the van der Waals forces. Unlike gravity, the van der Waals force has no preferred direction; therefore the contact force networks in 10 and 5 μm particle packings are more uniformly distributed in terms of magnitude and orientation. However, the F_n networks shown in Fig. 1(b) still reveal a strong force-chain pattern for all sized particles. The red lines in Fig. 1(b) represent the tensile (attractive) stress caused by the van der Waals force. For the packing of 1 mm particles, the van der Waals force is insignificant, so there is

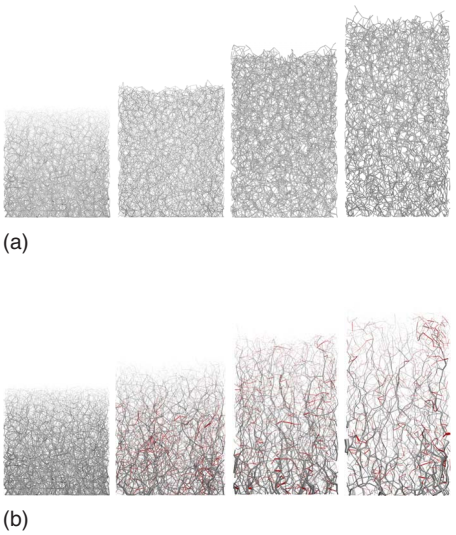

FIG. 1. (Color online) Distributions of (a) normal contact forces and (b) total normal forces in the packing of different sized particles (from left; 1 mm, 50 μm, 10 μm, and 5 μm). The gray lines represent compressive forces and the red lines tensile forces. Line thickness is proportional to force magnitude.

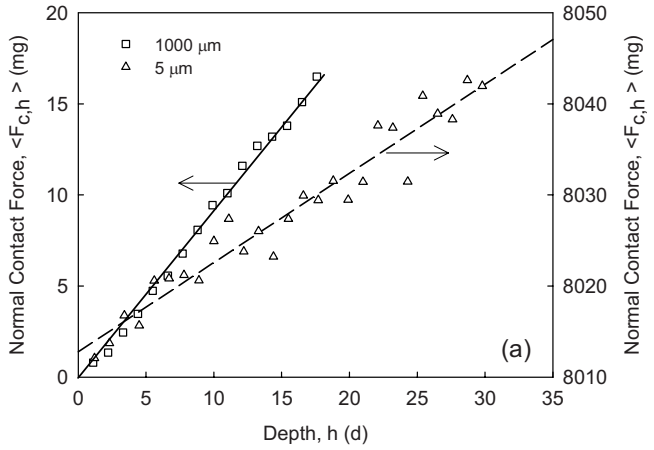

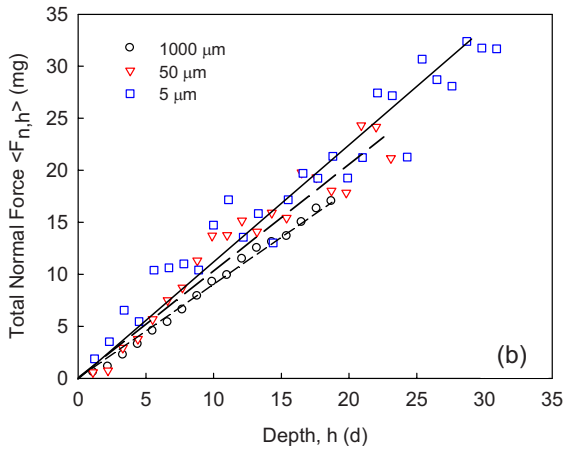

FIG. 2. (Color online) Mean depth-averaged (a) contact and (b) normal forces as a function of the packing depth h.

almost no tensile stress present. With decreasing particle size and hence increasing van der Waals force relative to particle weight, more tensile forces are present. Note that Fig. 1(b) looks more sparse than Fig. 1(a) because there is a large amount of small forces in Fig. 1(b) which are invisible in the plot.

As the packings are formed under gravity and are not symmetric in the vertical direction, it is important to know how the forces vary with packing height or depth. Figure 2 shows the mean F_c and F_n at a depth h below the top surface, $\langle F_{c,h}\rangle$ and $\langle F_{n,h}\rangle$, as a function of depth. $\langle F_{c,h}\rangle$ and $\langle F_{n,h}\rangle$ are obtained by summing up all the forces located within the layer of $\langle h, h+\delta h\rangle$ divided by the number of forces, and δh is equal to $1.1d$. Figure 2(a), indicates that, for the 1 mm particle packing, $\langle F_{c,h}\rangle$ starts from zero at the surface and increases linearly with h. The result is comparable with previous finding for noncohesive particles [5,12]. For the 5 μm particle packing, such a linear relationship still exists although the data are more scattered and start from a nonzero value due to the van der Waals force. On the other hand, Fig. 2(b) shows that the depth-averaged total normal forces $\langle F_{n,h}\rangle$ start from zero for all the packings. They all increase linearly the depth, with the slope increasing slightly from 0.910 for 1000 μm particles to 1.113 for 5 μm particles. Note that the linear relations in Fig. 2 are observed in the packings formed

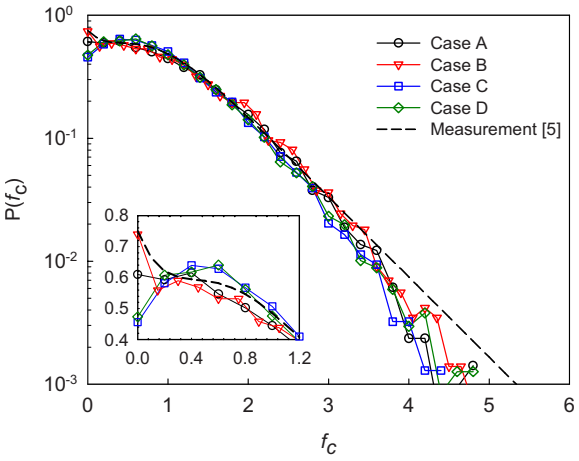

FIG. 3. (Color online) Distribution of the normalized contact forces for the packing of 1 mm particles with different material properties (see text for details of cases A–D). The inset is a linear plot of the distribution at small forces.

under periodic boundary conditions. If a frictional wall is present, then the stress-depth relation is described by the Janssen effect [30], i.e., the force increases linearly with depth initially but gradually becomes saturated as the vertical loading is supported by the particle-wall friction. It needs to be mentioned that, although the forces decrease with the packing height, the formed packings are homogeneous in structure except in the region near the bottom wall where the packing density varies due to the wall effect. This can be explained as follows. A tiny change of particle position (i.e., overlap between particles), although insignificant for the packing structure, is dramatically exemplified in the force structure because of the very large Young's modulus used to calculate the contact forces. This confirms the finding that force structure is a weighted function of packing structure and is much more sensitive than the packing structure itself [23].

To minimize the effect of gravity on the analysis of the force properties, in the following discussion, all forces are normalized by their corresponding depth-averaged values. A normalized parameter f is used, which is defined as the ratio of the force to the mean value at the same depth, $f = F^*/\langle F_h^*\rangle$, where F^* denotes F_c or F_n. To compare with the results in the literature [4,5,7,12], we first examined the distribution of the contact force in the 1 mm particle packing. In particular, we studied the effect of the material properties of the particles on the characteristics of the forces. We changed the properties of the 1 mm particles so that the particles were frictional with (without) the van der Waals force [denoted case A (B)], or frictionless with (without) the van der Waals force [case C (D)]. Figure 3 shows log-linear plots of the distributions of the normal contact forces $P(f_c)$ for the four cases. It can be observed that, for the packing of noncohesive frictional particles (case B), $P(f_c)$ exhibits an exponential decay at large forces and a plateau for $f_c < 1$ and a slight increase to 0.75 as forces approach zero. If the van der Waals force is present (case A), the distribution falls off more quickly at large forces, indicating that the van der Waals force, even though still very weak for 1 mm particles, has

made the forces more uniform by reducing the number of large forces. The force distributions for frictionless particles (cases *C* and *D*) are similar, both showing a well-defined peak at $f_c=0.5$ and a "dip" at small forces (see inset in Fig. 3). The changes are consistent with previous work [12] which suggested that the upturned tail at small forces is caused by the friction of the particles. Our results indicate that cohesion may also suppress the upturned tail if friction is present.

The present results are quite comparable with measured or simulated ones [5,12]. In particular, as shown in Fig. 3(a), $P(f_c)$ of case *B*, which is the packing of noncohesive, frictional particles, is very close to those measured from the surface of a packing of glass beads [5]. By fitting the data of case *B* with the empirical equation proposed by Mueth *et al.* [5],

$$P(f) = a(1 - be^{-f^2})e^{-cf}, \tag{3}$$

we obtained parameters a, b, and c of 3.20, 0.79, and 1.54, respectively, which are very close to the experimental results of (3.0, 0.75, 1.5) for a packing under large external loading [5]. There are differences between the simulated results and measured results at very large forces ($f_c>3$). Such a difference was also observed by Silbert *et al.* [12] and was attributed to the finite resolution of the experimental technique, which could not detect very small forces. By removing forces smaller than the particle weight, they observed that the agreement was improved. Another reason, which will be discussed further, is that small forces are more abundantly present internally than on the packing surfaces. As the experiments can only access the surface forces between particles and the wall, the measured data may not fully reflect the real forces within a packing.

Figure 4 plots the variations of $P(f_c)$ and $P(f_n)$ with particle size. Figure 4(a) shows that for 1 mm particles $P(f_c)$ has a plateau when the forces are less than the mean value ($f_c=1$). For 100 μm particles, $P(f_c)$ is a right-skewed distribution with a well-defined peak around $f_c=0.8$. As the particle size decreases, the peak of the plot becomes more prominent and moves closer to the mean value. The whole plot also moves to a narrower and more symmetrical form. We observed that $P(f_c)$ at large forces can be fitted well by an exponential distribution for 1 mm and 100 μm particles, although they have different rates of decrease. As particle size decreases to less than 10 μm, $P(f_c)$ at large forces departs from the exponential distribution and falls off more quickly. This is quite similar to observations for the packing of particles under large deformation [15,16]. This is not coincident since both cohesive forces and large external forces cause the contact forces to become more uniform by reducing the relatively large forces. At small forces, $P(f_c)$ for the packings of particles smaller than 100 μm (i.e., cohesive particles) shows a similar pattern to that observed in the study of cohesive granular materials during the shearing process [18].

Interestingly, the distributions of the total normal forces in Fig. 4(b) show an opposite trend: $P(f_n)$ becomes wider as particle size decreases. The negative values in the figure represent the attractive (tensile) forces between particles. $P(f_n)$

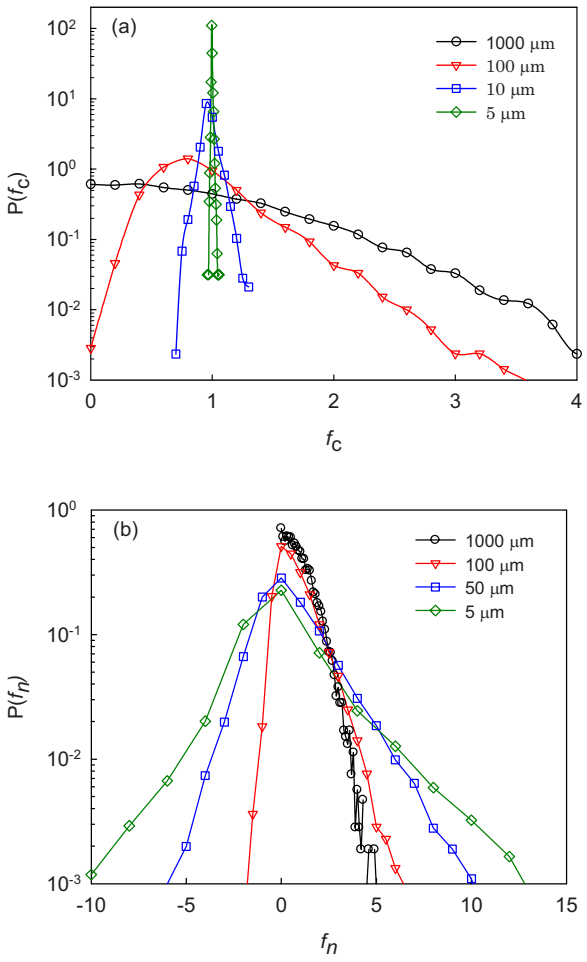

FIG. 4. (Color online) Distributions of the normalized (a) contact forces and (b) total forces in the packings of different sized particles. Default values in Table I were used.

in the 1 mm particle packing are positive with an exponential tail at large forces and a plateau at small forces. When particle size decreases and the van der Waals force plays a more important role, more tensile forces are present so the distributions show a single-modal curve with a peak around $f_n=0$. The distributions also become broader and the exponential falloff extends to the peak for 50 μm or smaller particles. Richefeu *et al.* [25] also observed a similar trend in their packings of wet particles in which the cohesion between particles is caused by capillary forces. This is because the cohesive forces in the packing of fine particles become dominant over gravity and the contact forces mainly respond to the cohesion but not gravity. So there are abundant small forces as the contact force and the van der Waals force balance each other.

The effect of particle size on force structure can be further observed from the force orientation pattern. Figure 5 shows the angle distribution of the normal total force $P(\theta)$ for different particle sizes, where θ is the angle between the force and the vertical direction with $\theta \in (0°, 90°]$. It clearly illustrates the anisotropy of the force network. For the 1 mm particle packing, the distribution shows two peaks at 60° and 90°, indicating more forces close to the horizontal than close to the vertical direction due to the effect of gravity. This

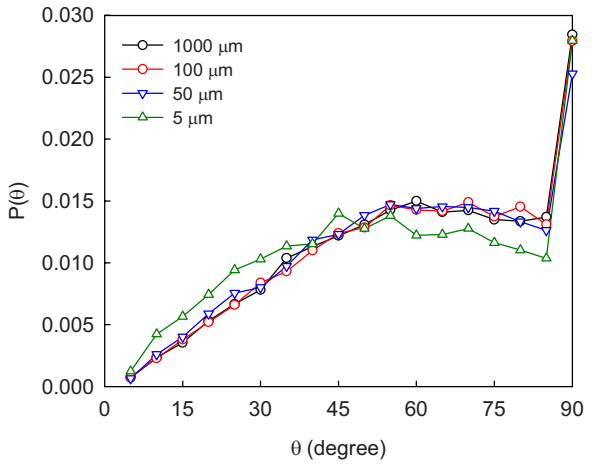

FIG. 5. (Color online) Orientational distribution of the normal force in packings of different particle sizes. Here θ is the angle between the force direction and the vertical.

trend becomes less obvious as the particle size decreases. For the 5 μm particle packing, the first peak appears at 45°, which reflects the increasing role of the van der Waals force as particle size decreases. Note that the normal contact forces have orientation patterns similar to those of the normal forces, so they are not shown here. Separate plots of the angle distributions of tensile and compressive forces indicate a similar pattern.

So far, it is still unclear if spatial correlations exist for the interparticle forces. While some experimental work shows no [5] or weak [7] correlation, other work indicated that correlation does exist [12] for a short range (typically within 2–3 particle diameters). A function $\phi(f)$ was proposed to characterize the correlation between the neighboring forces, given by [5,7,31]

$$\phi(f) = \frac{\Sigma_i \Sigma_{j>i} \delta(|r_{ij} - r|) f_i f_j}{\Sigma_i \Sigma_{j>i} \delta(|r_{ij} - r|)}, \tag{4}$$

where r_{ij} is the distance between contact points i and j. Figure 6 shows the correlations of normal contact forces $\phi(f_c)$ and normal total forces $\phi(f_n)$ based on the present results. $\phi(f_c)$ in Fig. 6(a) shows that the 1 mm particle packing has two strong peaks at $r=0.9d$ and $1.8d$, respectively, indicating that a correlation exists for a radial distance extending to a couple of particle diameters. Both peaks decrease as particle size decreases, suggesting weakening correlation. $\phi(f_c)$ is almost flat for the 5 μm particle packing, which indicates that no correlation exists and the force network is more localized. On the other hand, $\phi(f_n)$ in Fig. 6(b) shows that the correlation still exists for the normal total force for all sized particles within a couple of particle diameters. Note that the averaged magnitudes of $\phi(f_n)$ vary significantly from around 1 for 1 mm particles to more than 100 for 100 μm particles. So, for clarity, all the curves in Fig. 6(b) have been normalized against their corresponding peak values. The negative values in $\phi(f_n)$ are due to the presence of tensile forces. If only the magnitudes of the forces are used to calculate the force correlation, then two peaks can be observed for fine particles within a distance of one particle diameter, as shown

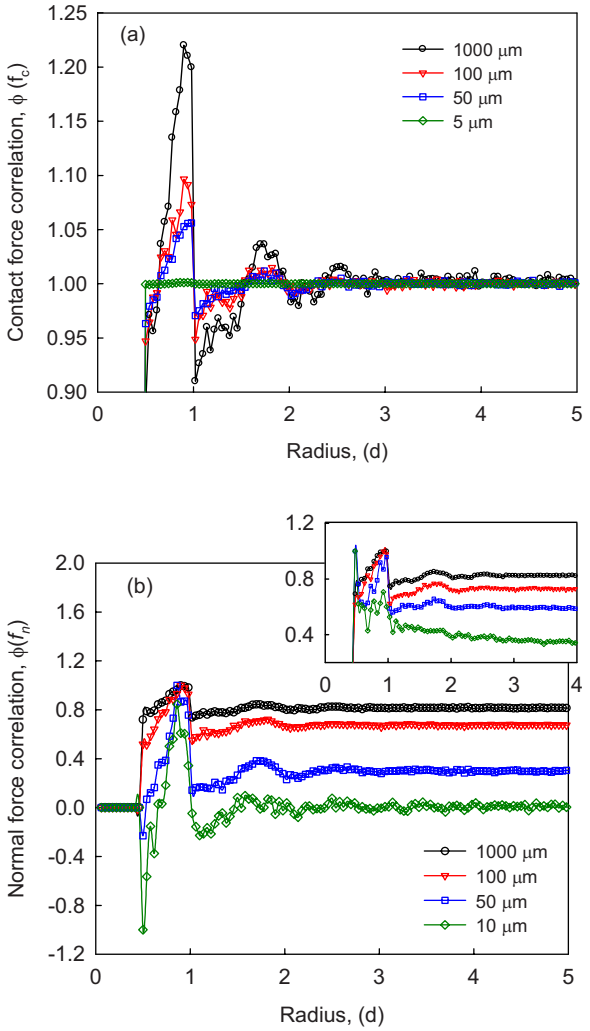

FIG. 6. (Color online) Spatial correlations of (a) normal contact force and (b) normal total force for packings of different sized particles. The inset shows the correlation when only the magnitudes of the forces are used. For clarity, all the curves in (b) are normalized against their corresponding peak values, which are 1.22, 1.45, 3.09, and 85.04 for 1000, 100, 50, and 10 μm particles, respectively.

in the inset of Fig. 6(b). As the particle size decreases, the first peak at $r=(1/2)d$ becomes more prominent while the peak at $r=d$ becomes weaker. Therefore, our results indicate that, under the current packing conditions, spatial correlation of forces exists for noncohesive particles. As the cohesion between particles gets stronger, such correlation becomes weaker for the contact forces but still exists for the total normal forces.

It is well known that the pressure in a liquid is isotropic and proportional to the depth below its surface. This hydrostatic property is often not available for granular materials [3]. This can be illustrated by two well-known examples. First, the pressure under the center of a sandpile can be a local minimum [3], and second, the pressure in a silo is depth independent below a certain depth [30]. However, this nonhydrostatic property for granular materials may be simply caused by the external effect from, e.g., the bottom wall in

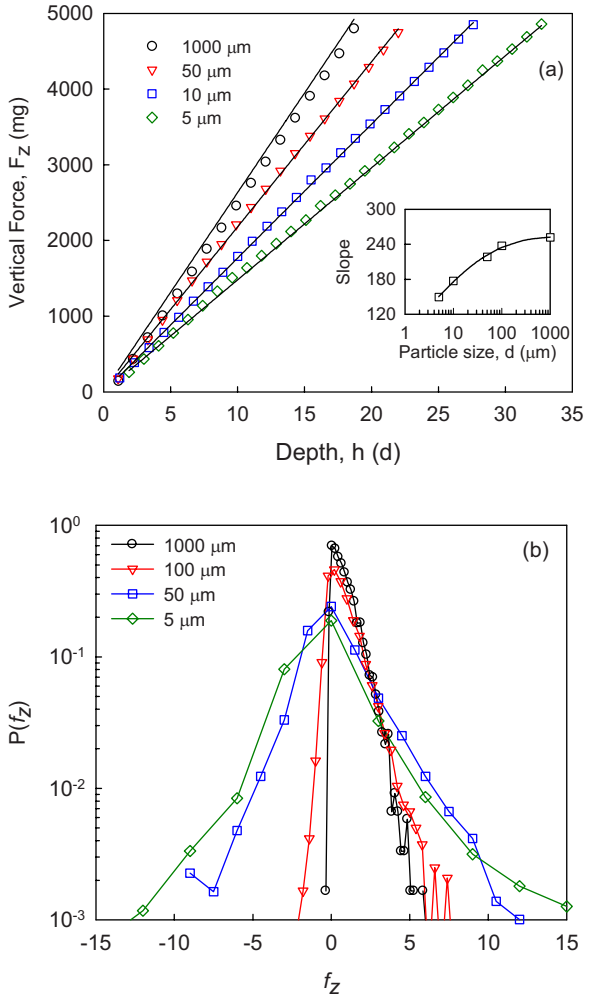

FIG. 7. (Color online) (a) Mean total forces in the vertical direction as a function of the depth from the top surface of a packing (the inset shows the variation of linear slope with the particle size); (b) distributions of the normalized forces on a plane for different sized particles.

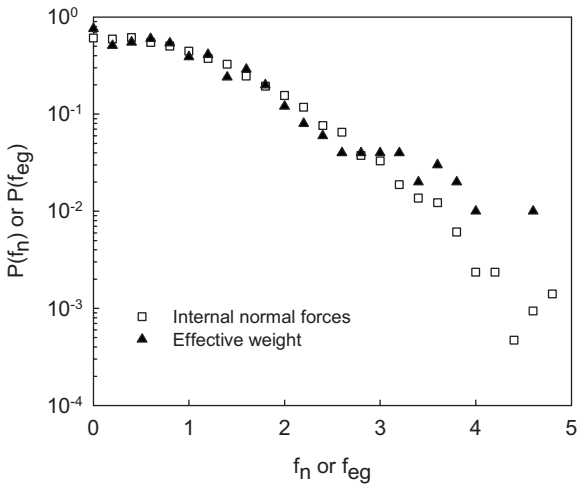

FIG. 8. Distribution of the normalized internal normal force and effective weight for the packing of 1 mm particles. Default values in Table I are used.

piling or the sidewall in a silo. As our packings were formed under periodic boundary conditions, there are no sidewalls. To study the variation of the force with depth under this condition, we defined the total normal forces on an imaginary plane as [32]

$$F_z = \sum (\mathbf{F}_{n,ij})_z \tag{5}$$

where $\mathbf{F}_{n,ij}$ are the normal forces between particles i and j and passing through the plane, and z denotes the vertical component of the forces. Note the net force in the horizontal directions (XY plane) should be equal to zero. We plot in Fig. 7 the forces on planes at different depths as a function of the depth. We observe that the height-averaged value F_z and z follow a strict linear relationship for all the packings as shown in Fig. 7(a). This demonstrates that, in the absence of wall, the particle packing, exhibits the hydrostatic property like a liquid in the vertical direction. Note that the slope decreases with particle size, as shown in the inset in Fig. 7(a). As the slope relates to the bulk density of a packing, the decrease of slope for small particles indicates the decreasing role of gravity. Figure 7(b) shows the distributions of the normalized forces on the plane, $P(f_z)$. The positive values mean the compressive forces from the particles above (the same direction as gravity), and the negative values represent the tensile forces (opposite to gravity). Note that Fig. 7(b) is the force distribution in the z direction, but it has a similar pattern to the total force distribution in three dimensions as shown in Fig. 4(b). Such similarity indicates that the force distributions are the same in three directions.

It should be noted that, while people are mostly interested in the force structure within a packing, most of the experimental techniques thus far reported in the literature can only measure the surface forces between particles and walls except for a few studies with two-dimensional systems [9,33] or using confocal fluorescence microscopy techniques [34,35]. In general, internal particle-particle forces and external particle-wall forces are different, so it may not be always correct to use the external forces to infer the internal ones. To establish a link between the external and the internal forces, Snoeijer *et al.* [13] proposed the so-called effective weight, defined as

$$F_{eg,i} = m_i g + \sum_j (\mathbf{F}_{ij})_z, \tag{6}$$

where j is the particle contacting particle i from above, and z denotes the vertical component of all "upper" contact forces. To distinguish the contact force from the effective weight, they performed two-dimensional numerical simulations of the packing of frictionless particles. Their results showed that the effective weight is strongly affected by the contact geometry and the contact forces are more robust. In general the forms of $P(f_{eg})$ on the container surface and $P(f_c)$ in the packing are different. Figure 8 shows the internal normal force distribution $P(f_n)$ and the distribution of the forces acting on the container bottom, $P(f_{eg})$, which is the effective weight of the first-layer particles and usually measured in experiments [5,7]. The two distributions are similar except

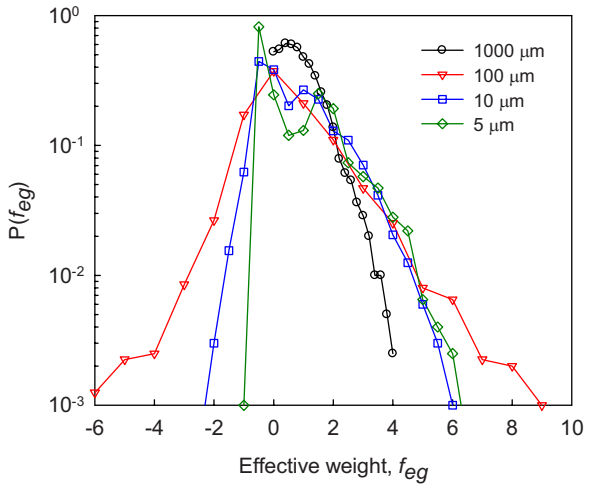

FIG. 9. (Color online) Distribution of the normalized effective weight for the packings of different sized particles.

for very small or large forces. While $P(f_{eg})$ shows an upturning tail at small forces, such an upturn is significantly suppressed in $P(f_n)$. Instead a plateau is shown in $P(f_n)$ as the forces approach zero due to the van der Waals force. On the other hand, $P(f_n)$ falls off more quickly than $P(f_{eg})$ at large forces. As discussed earlier, this means that, there are more abundant small forces within a packing than those acting on the packing surface.

The difference between the two types of force can be more clearly demonstrated in Fig. 9 which shows the distribution of the effective weights acting on individual particles within a packing. The most striking feature revealed in the figure is that the single-modal distributions for the 1 mm and 100 μm particle packings become bimodal when the particle size is less than 10 μm. Comparing with $P(f_n)$ in Fig. 4(b), the two distributions for the relatively large particles (1 mm and 100 μm) are still similar, but not so for the fine particles ($d<10$ μm). Therefore, the internal force structure of fine particle packing cannot be measured from outside in the same way as for coarse particles. It is also interesting to note that the two peaks observed in each side correspond to downward (compressive) and upward (tensile) forces, which indicates that two phases may exist in the packings, governed by the compressive and tensile stress.

IV. CONCLUSIONS

We performed a numerical investigation of the interparticle forces in the packing of fine, cohesive particles, focusing mainly on the characteristics of the normal contact force and normal total force varying with particle size. Our results indicated that the cohesion between particles significantly affects the force structure. The main findings can be summarized as follows.

(1) Despite the homogeneous packing structures, the force structures are asymmetric due to the effect of gravity, propagating from bottom to top. Both the average normal contact force and the total force increase linearly with depth in the absence of lateral walls.

(2) As particle size decreases, the contact forces become more uniform but less aligned with the vertical direction, and their distribution becomes narrower and more symmetric. On the other hand, the total normal forces have more tensile (attractive) forces as the cohesion between particles increases, although they have smaller magnitudes than the compressive forces.

(3) The forces are correlated spatially for a radial distance extending to a couple of particle sizes. As particle size decreases, the correlation of the normal contact forces becomes weaker.

(4) The internal force structures are different from those measured on the external surface, as highlighted by the effective weight. The bimodal distribution of the effective weight in the fine particle packings suggests there may exist two phases in the packings, governed by the compressive and tensile stresses.

ACKNOWLEDGMENTS

The authors are grateful to the Australia Research Council (ARC) and CSIRO for the financial support of this work.

[1] *Granular Matter: An Interdisciplinary Approach*, edited by A. Mehta (Springer-Verlag, New York, 1994).
[2] H. M. Jaeger, S. R. Nagel, and R. P. Behringer, Rev. Mod. Phys. **68**, 1259 (1996).
[3] P. G. de Gennes, Rev. Mod. Phys. **71**, s374 (1999).
[4] C.-H. Liu, S. R. Nagel, D. A. Schecter, S. N. Coppersmith, S. Majumdar, S. Narayan, and T. A. Witten, Science **269**, 513 (1995).
[5] D. M. Mueth, H. M. Jaeger, and S. R. Nagel, Phys. Rev. E **57**, 3164 (1998).
[6] D. Howell, R. P. Behringer, and C. Veje, Phys. Rev. Lett. **82**, 5241 (1999).
[7] G. Løvoll, K. J. Måløy, and E. G. Flekkøy, Phys. Rev. E **60**, 5872 (1999).
[8] D. L. Blair, N. W. Mueggenburg, A. H. Marshall, H. M. Jaeger, and S. R. Nagel, Phys. Rev. E **63**, 041304 (2001).
[9] T. S. Majmudar and R. P. Behringer, Nature (London) **435**, 1079 (2005).
[10] K. Liffman, D. Y. C. Chan, and B. D. Hughes, Powder Technol. **72**, 255 (1992).
[11] F. Radjai, M. Jean, J. Moreau, and S. Roux, Phys. Rev. Lett. **77**, 274 (1996).
[12] L. E. Silbert, G. S. Grest, and J. W. Landry, Phys. Rev. E **66**, 061303 (2002).
[13] J. H. Snoeijer, M. van Hecke, E. Somfai, and W. van Saarloos, Phys. Rev. E **67**, 030302(R) (2003).
[14] C. S. O'Hern, S. A. Langer, A. J. Liu, and S. R. Nagel, Phys. Rev. Lett. **88**, 075507 (2002).

[15] H. A. Makse, D. L. Johnson, and L. M. Schwartz, Phys. Rev. Lett. **84**, 4160 (2000).
[16] A. H. W. Ngan, Phys. Rev. E **68**, 011301 (2003).
[17] L. E. Silbert, A. J. Liu, and S. R. Nagel, Phys. Rev. E **73**, 041304 2006.
[18] S. J. Antony, Phys. Rev. E **63**, 011302 (2000).
[19] S. N. Coppersmith, C.-h. Liu, S. Majumdar, O. Narayan, and T. A. Witten, Phys. Rev. E **53**, 4673 (1996).
[20] J. H. Snoeijer, T. J. H. Vlugt, M. van Hecke, and W. van Saarloos, Phys. Rev. Lett. **92**, 054302 (2004).
[21] M. E. Cates, J. P. Wittmer, J.-P. Bouchaud, and P. Claudin, Phys. Rev. Lett. **81**, 1841 (1998).
[22] T. Unger, J. Kertesz, and D. E. Wolf, Phys. Rev. Lett. **94**, 178001 (2005).
[23] C. S. O'Hern, S. A. Langer, A. J. Liu, and S. R. Nagel, Phys. Rev. Lett. **86**, 111 (2001).
[24] V. Trappe, V. Prasad, L. Cipelletti, P. N. Segre, and D. A. Weitz, Nature (London) **411**, 772 (2001).
[25] V. Richefeu, F. Radjai, and M. S. El Youssoufi, Eur. Phys. J. E **21**, 359 (2006).
[26] F. A. Gilabert, J.-N. Roux, and A. Castellanos, Phys. Rev. E **75**, 011303 (2007).
[27] R. Y. Yang, R. P. Zou, and A. B. Yu, Phys. Rev. E **62**, 3900 (2000).
[28] R. Y. Yang, R. P. Zou, and A. B. Yu, AIChE J. **49**, 1656 (2003).
[29] R. Y. Yang, R. P. Zou, and A. B. Yu, J. Appl. Phys. **94**, 3025 (2003).
[30] H. A. Janssen, Z. Ver. Dtsch. Ing. **39**, 1045 (1895).
[31] L. E. Silbert, D. Ertas, G. S. Grest, T. C. Halsey, and D. Levine, Phys. Rev. E **65**, 031304 (2002).
[32] *Mechanics of Granular Materials—An Introduction*, edited by M. Oda and K. Iwashita (Balkema, Rotterdam, 1999).
[33] J. F. Geng, G. Reydellet, E. Clement, and R. P. Behringer, Physica D **182**, 274 (2003).
[34] J. Brujic, S. F. Edwards, I. Hopkinson, and H. A. Makse, Physica A **327**, 201 (2003).
[35] J. Zhou, S. Long, Q. Wang, and A. D. Dinsmore, Science **312**, 1631 (2006).